Dissociated cortical phase- and amplitude-coupling patterns in the human brain

Marcus Siems[1,2] and Markus Siegel[1]

[1]Centre for Integrative Neuroscience and MEG Center, University of Tübingen, Germany

[2] IMPRS for Cognitive and Systems Neuroscience, University of Tübingen, Germany

Contact Information

Correspondence: marcus.siems@uni-tuebingen.de & markus.siegel@uni-tuebingen.de

Abstract

Coupling of neuronal oscillations may reflect and facilitate the communication between neuronal populations. Two primary neuronal coupling modes have been described: phase-coupling and amplitude-coupling. Theoretically, both coupling modes are independent, but so far, their neuronal relationship remains unclear. Here, we combined MEG, source-reconstruction and simulations to systematically compare cortical phase-coupling and amplitude-coupling patterns in the human brain. Importantly, we took into account a critical bias of amplitude-coupling measures due to phase-coupling. We found differences between both coupling modes across a broad frequency range and most of the cortex. Furthermore, by combining empirical measurements and simulations we ruled out that these results were caused by methodological biases, but instead reflected genuine neuronal amplitude coupling. Overall, our results suggest that cortical phase- and amplitude-coupling patterns result from distinct neural mechanisms. Furthermore, our findings highlight and clarify the compound nature of amplitude coupling measures.

Introduction

The brain is a distributed information processing system. Correlated oscillations of neuronal activity have been proposed to facilitate and orchestrate communication between distant brain regions (Singer, 1999; Siegel et al., 2012; Fries, 2015). In this context, neuronal firing is described as a probabilistic process that is shaped by the phase and amplitude of oscillatory rhythms (Destexhe et al., 1999; Engel et al., 2001; Siegel et al., 2012; Hillebrand et al., 2012; Hipp et al., 2012; Engel et al., 2013; Jahnke et al., 2014; Fries, 2015; Jensen and Mazaheri, 2010). When temporally correlated, co-fluctuations of local oscillations may enhance effective communication between neuronal populations and enable the multiplexing of neuronal information (Akam and Kullmann, 2014; Lopes da Silva, 2013; Singer, 2013). There are two primary coupling modes between neuronal oscillations: phase-coupling and amplitude-coupling (Bruns et al., 2000; Siegel et al., 2012; Engel et al., 2013).

Phase-coupling refers to a consistent phase-alignment between neuronal oscillations, which may reflect a frequency specific signature of neuronal interactions (Siegel et al., 2012). Moreover, phase-coupling may itself modulate effective connectivity by aligning rhythmic excitability fluctuations to rhythmic spike inputs (Fries, 2015). Consistent with this functional role, long-range neuronal phase-coupling reflects various cognitive processes, such as e.g. selective attention (Bosman et al., 2012; Buschman and Miller, 2007; Gregoriou et al., 2009; Siegel et al., 2008), perception (Hipp et al., 2011), memory (Fell and Axmacher, 2011; Palva et al., 2010) and task switching (Buschman et al., 2012). Task-dependent phase-coupling is expressed in well-structured large-scale cortical networks (Hipp et al., 2011; Palva et al., 2010).

Amplitude-coupling refers to the temporal co-modulation of the amplitude (or power) of neuronal oscillations. Like phase-coupling, amplitude-coupling may not only result from,

and thus reflect, neuronal interactions, but may also regulate these interactions by temporally aligning distant processes associated with fluctuating oscillations (Siegel et al., 2012; von Nicolai et al., 2014). Also amplitude-coupling is expressed in well-structured cortical networks that match known anatomical and functional connectivity (Hipp et al., 2012; Siems et al., 2016), resemble fMRI correlation patterns (Brookes et al., 2011; Deco and Corbetta, 2011; Destexhe et al., 1999; Hipp and Siegel, 2015; Mantini et al., 2007; Nir et al., 2008; O'Neill et al., 2015), and are more stable than phase-coupling networks (Colclough et al., 2016; Wang et al., 2014). Amplitude-coupling is largely driven by amplitude dynamics below 0.1 Hz (Hipp et al., 2012), which may reflect the slow establishment and decay of communicating networks (Destexhe et al., 1999; Leopold et al., 2003; Mantini et al., 2007; Larson-Prior et al., 2011; Hipp et al., 2012; Engel et al., 2013).

Both coupling modes may provide versatile biomarkers for various neuropsychiatric diseases (Fornito et al., 2015; Stam, 2014; Uhlhaas and Singer, 2012) including autism (Kitzbichler et al., 2015), schizophrenia (Cetin et al., 2016; Maran et al., 2016), epilepsy (Burns et al., 2014; van Dellen et al., 2014; Zerouali et al., 2016), dementia (Koelewijn et al., 2017; Maestú et al., 2015), Parkinson's disease (Oswal et al., 2016), multiple sclerosis (Cover et al., 2006; Schoonheim et al., 2013; Tewarie et al., 2014) and blindness (Hawellek et al., 2013).

Despite the strong interest and rapidly growing evidence on both, neuronal phase- and amplitude coupling, their relationship remains unclear. In principle, both coupling-modes could be independent. There could be phase-coupling without amplitude-coupling and vice versa (Siegel et al., 2012). In that case amplitude- and phase-coupling might serve distinct roles and indicate separable neuronal mechanisms. Alternatively, both coupling modes may be tightly linked, e.g. if both modes reflect the same underlying neuronal interactions, or if one coupling mode causes the other. The central aim of this study was

to non-invasively investigate this relationship between phase- and amplitude coupling in the human brain with MEG.

Addressing this question is complicated by a methodological peculiarity of the estimation of amplitude coupling that has recently been pointed out (Palva et al., 2018). If spurious coupling due to field-spread is suppressed by orthogonalization (Brookes et al., 2012; Hipp et al., 2012), measures of amplitude coupling are also partially sensitive to phase coupling (Palva et al., 2018). In other words, the measured amplitude-coupling reflects a mixture of the genuine, i.e. physiological amplitude-coupling of interest and a bias due to phase-coupling.

Thus, we approached our central question in two steps. First, we tested if there is a physiological component to the cortical amplitude-coupling measured with MEG, beyond the phase-coupling bias. Second, we addressed our main question how physiological phase- and amplitude-coupling relate. To this end, we systematically compared the cortical correlation structure of both coupling modes across the human brain.

Results

We quantified brain-wide neuronal phase- and amplitude-coupling from resting-state MEG measurements in 95 healthy participants. We applied source-reconstruction (Van Veen et al., 1997) to systematically characterize neuronal coupling at the cortical source level. Field spread (or signal leakage) can induce spurious coupling of sensor- and source-level MEG/EEG signals. Thus, we employed two coupling measures discounting signal leakage. For phase-coupling, we applied the weighted phase lag index (wPLI; Nolte et al., 2004; Vinck et al., 2011)

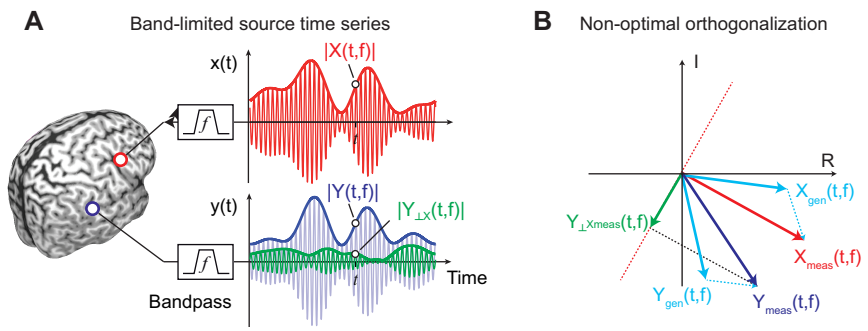

Figure 1. Principle of signal leakage reduction for amplitude relations

(A) Illustration of band-limited time series from two sources X (red, upper panel) and Y (blue, middle panel) with their envelopes (thick lines). The green thick line resembles the envelope of signal Y orthogonalized on signal X. (B) illustrates how the orthogonalization can induce specious amplitude coupling in the presence of phase coupling and signal leakage. We orthogonalize the measures signal Y_{meas} onto the measured signal X_{meas}. In the presence of signals leakage, both measured signals reflect a mix of the genuine signals X_{gen} and Y_{gen}. For non-zero phase coupling between X_{gen} and Y_{gen}, X_{meas} is rotated away from X_{gen}. This causes sub-optimal signal orthogonalization.

(see Fig. S2 for comparison with other phase-coupling measures). For amplitude coupling, we employed pair-wise signal orthogonalization before estimating amplitude-correlations (Fig. 1A) (Brookes et al., 2012; Hipp et al., 2012).

It has recently been shows that signal orthogonalization does not perfectly discount volume conduction in the presence of genuine phase coupling with non-zero phase delays (Fig. 1B) (Palva et al., 2018). Intuitively, this is because, in the presence of signal leakage, such phase-coupling systematically rotates the estimate of the signal to which one aims to orthogonalize, which results in sub-optimal orthogonalization and spurious amplitude-correlations. To test if the empirically measured amplitude-correlations reflect this bias we directly estimated this bias with data simulations based on the same measurements (see 2.6).

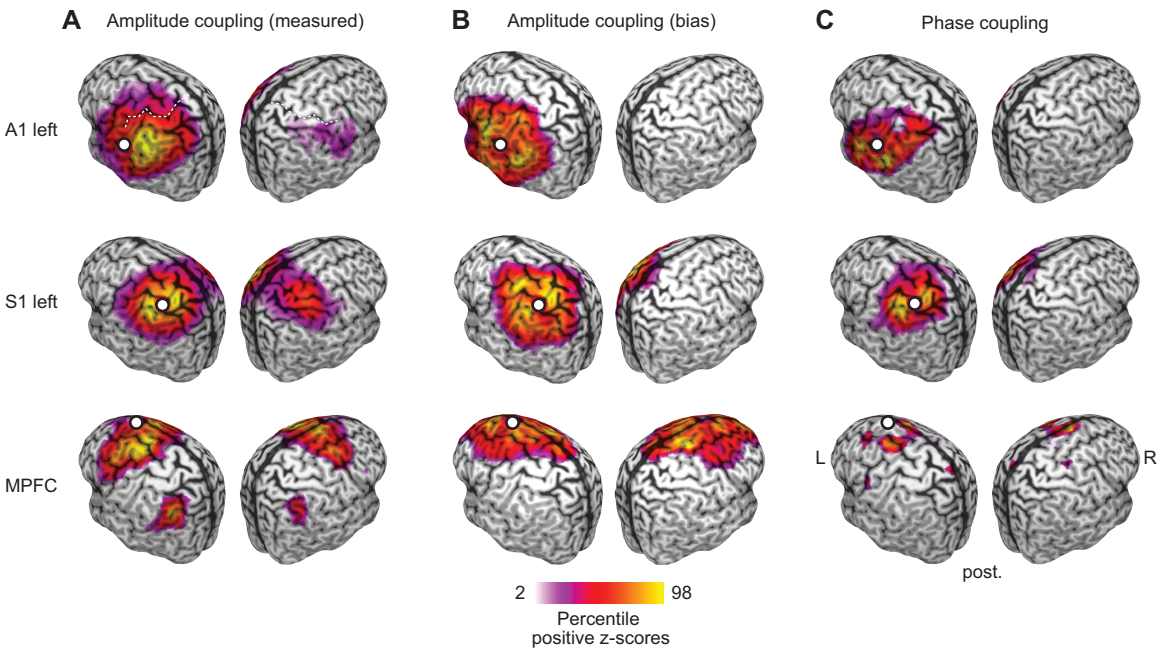

Figure 2. Seed based analysis for early sensory and higher order cortices at 16Hz

Seed-based correlation structure (z-scores) of the left auditory (left A1, top panel), left somatosensory (left S1, middle panel), and the medial prefrontal cortex (MPFC, bottom panel) for measured amplitude-coupling (A), amplitude-coupling bias (B) and phase coupling (C). Coupling z-scores are tested against zero and statistically masked ($p<0.05$, FDR corrected). Color scale ranges from the 2nd to the 98th percentile of significant values, scaled within each panel. White dots indicate seed regions. The white dashed line in the top left panel highlights the central sulcus (see 2.3 for exact seed coordinates).

In brief, for each subject, we simulated cortical signals given their measured phase coupling (wPLI) for a worst-case scenario of 90 º phase-shift and their measured signal leakage (resolution matrix). With this approach we quantified the expected bias in amplitude coupling if there was no genuine amplitude coupling.

Seed-Based Connectivity Analysis

As a first step, we performed a seed-based analysis (Fig. 2). We computed cortex-wide phase- (Fig. 2C) and amplitude-coupling (Fig. 2A) patterns of neural activity at 16 Hz for several early sensory and higher order cortical regions, for which we expected robust

coupling patterns. As early sensory regions we chose primary auditory (A1) and somatosensory cortex (S1), which show strong inter-hemispheric connectivity and robust amplitude-coupling patterns at 16 Hz (Hipp et al., 2012; Mehrkanoon et al., 2014; Siems et al., 2016). For each seed, subject and both coupling modes, we z-scored the raw coupling measures and tested for z-scores larger than zero across subjects (FDR-corrected). This revealed which connections showed significant above-average coupling, while discounting global offsets of coupling measures (Hipp et al., 2012, p. 2012).

For both sensory seeds (A1 and S1), amplitude coupling was strongest to regions surrounding the seed region and to the homologous area in the other hemisphere (Fig. 2 left & right). Phase coupling did not show this pattern, but only above-average connectivity surrounding the seed.

Our findings for a higher order seed region confirmed these results. We investigated phase and amplitude coupling for the medial prefrontal cortex (MPFC, Fig. 2 bottom row), which shows a complex connectivity structure for amplitude coupling at 16 Hz (Hipp et al., 2012; Siems et al., 2016). We found that amplitude coupling of MPFC peaked bilaterally in the dorsal prefrontal and lateral parietal cortices. In contrast, phase coupling only peaked surrounding the seed region.

The amplitude-coupling bias (Fig. 2B) did not resemble the complex spatial structure of the measured amplitude coupling. In contrast, it showed a stereotypical and robust pattern of above-average connectivity only to sources near the seed independent of the seed location.

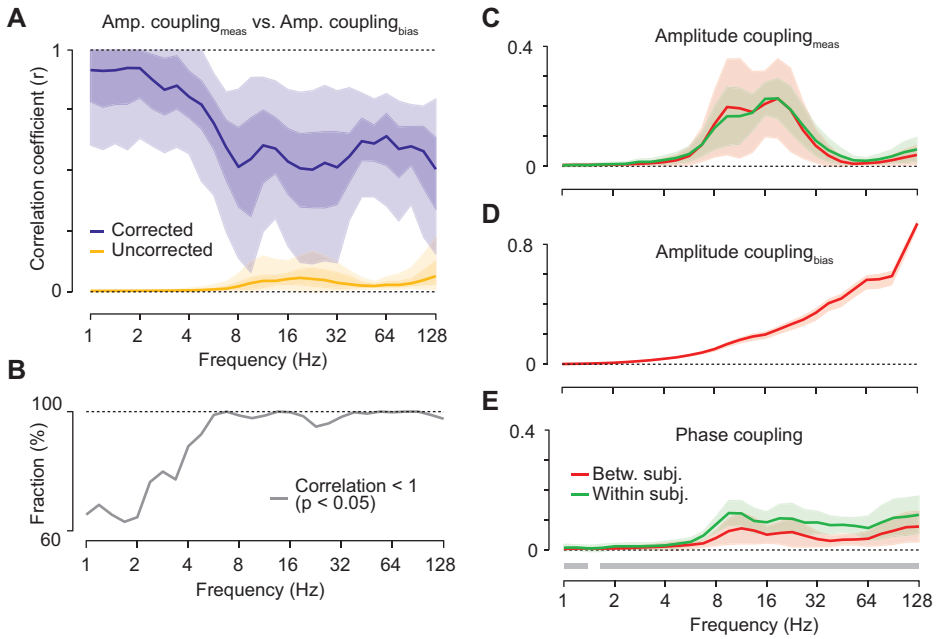

Figure 3. Correlation between measured and biased amplitude-coupling patterns

(A) Frequency resolved correlation between amplitude- and biased coupling patterns. Lines depict the median corrected (blue) and uncorrected (yellow) correlation. Shaded areas indicate the 5-95% and 25-75% interpercentile range over space. (B) Fraction of cortical locations that show significant ($p<0.05$, FDR-corrected) genuine amplitude coupling, i.e. a correlation between the measured amplitude coupling and the biased coupling that, corrected for the signal-to-noise ratio, is significantly smaller than 1 (see 2.9). (C) Reliability of measured amplitude-coupling patterns within (green) and between (red) subjects. Shaded areas indicate the 25-75% interquartile range. (D) Reliability of amplitude-coupling bias patterns between subjects. (E) Reliability of phase-coupling patterns within (green) and between (red) subjects. The gray bars below the lines indicates significantly larger reliability within as compare to between subjects ($p<0.05$, FDR-corrected).

Physiological amplitude coupling

To quantitatively address our first question, i.e. if the measured amplitude coupling reflects genuine physiological amplitude coupling, we systematically assessed the similarity of the bias and measured amplitude across the entire cortex and for all

frequencies (Fig. 3). A high correlation would indicate that the measured amplitude coupling can largely be explained by the amplitude-coupling bias. Conversely, the fraction of non-explained amplitude coupling can be attributed to genuine amplitude coupling.

For each frequency and both measures, we computed the coupling between all cortical regions, i.e. we computed the full connectivity matrices of the measured cortex-wide amplitude coupling and its bias. We then correlated the patterns of bias and measured amplitude coupling for each cortical seed region (3 examples from the 457 sources are shown in Fig. 2). In other words, we correlated each column of the connectivity matrices between measures. Averaged across all seed regions, this revealed a positive correlation that markedly peaked from 8-32 Hz and above 90Hz with median correlation coefficients below 0.1 (Fig. 3A, yellow line).

At first sight, the low correlation between measured and bias amplitude coupling, suggest that there is indeed genuine amplitude coupling. However, it is important to realize that the correlation between two measures does not only reflect their true underlying correlation, but also the measures' signal-to-noise ratio or reliability (Bergholm et al., 2010; Hipp et al., 2012; Siems et al., 2016; Spearman, 1904). Even for a perfect match between the bias and measured amplitude coupling, those areas and frequencies with lower signal-to-noise ratio will show a lower correlation between patterns than areas or frequencies with higher signal-to-noise ratio. Thus, the observed low and frequency specific correlation between the patterns may merely reflect biases due to signal-to-noise and does not allow for directly inferring genuine amplitude coupling.

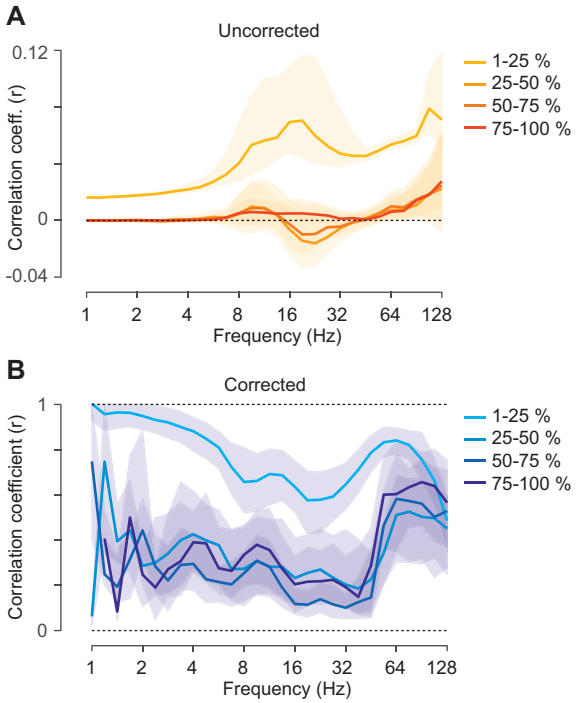

Figure 4. Correlation between measured and biased amplitude-coupling patterns for separate coupling distances

(A) Frequency resolved uncorrected correlation between amplitude- and biased coupling patterns for four coupling-distance quartiles. For the correlation between both measures, the patterns (columns of the adjacency matrix) were split into four quartiles depending on the distance of each source from the seed. Lines indicate median correlation. Shaded areas indicate the 25-75% interquartile range over space. (B) Frequency resolved attenuation corrected correlation between amplitude- and biased coupling patterns for four coupling-distance quartiles.

We applied attenuation correction of correlations (Hipp and Siegel, 2015; Siems et al., 2016; Spearman, 1904) to account for the effect of signal reliability. Attenuation corrected correlations quantify how strong a correlation would be for perfectly reliable signals (Fig. S1). We employed the between-subject reliability (correlation) of measured amplitude and bias coupling patterns as a proxy for each measure's reliability (Hipp and Siegel, 2015; Siems et al., 2016). For the measured amplitude coupling, between-subject reliability peaked around 16 Hz (Fig. 3C) compatible with previous findings (Hipp

and Siegel, 2015; Siems et al., 2016). For the bias, reliability increased monotonically with frequency (Fig. 3D), which is likely due to the decreasing spatial resolution of beamforming filters with increasing frequency.

We corrected the correlation between the measured and bias amplitude coupling patterns for these reliabilities by pooled division (see 2.8). This correction had a marked effect (Fig. 3A, blue line). As predicted, the overall correlation between measured amplitude coupling patterns and the bias patterns increased. The median attenuation corrected correlation was around 0.85 for frequencies below 5 Hz and around 0.5 for higher frequencies. This suggests that, for frequencies above 5 Hz, on average more than 70 % of the variance in the measured amplitude-coupling patterns is due to physiological amplitude coupling.

The positive correlation between bias and measured amplitude coupling may not only reflect non-optimal orthogonalization, but also a true similarity between these patterns. Nearby sites may show genuinely higher amplitude correlations similar to the stereotypical pattern of the amplitude-coupling bias that reflects nearby field-spread and phase-coupling (compare Fig. 2C). In contrast, more complex patterns in amplitude coupling display a non-monotonous distance relation (for example Fig. 2 MPFC). To investigate this, we split each seed correlation-pattern in four distance quartiles and repeated our analysis separately, for each quartile (Fig. 4). As hypothesized, we found that the similarity between the bias and the measured amplitude coupling increased for the closest connections. For larger distances, the correlation decreased with stronger dissimilarity between the bias and measured amplitude coupling up to 64Hz.

We next sought to statistically assess if attenuation corrected correlations were indeed smaller than 1, i.e. if there is any physiological amplitude coupling. The attenuation corrected correlation is an unbiased estimate (Figure S1).

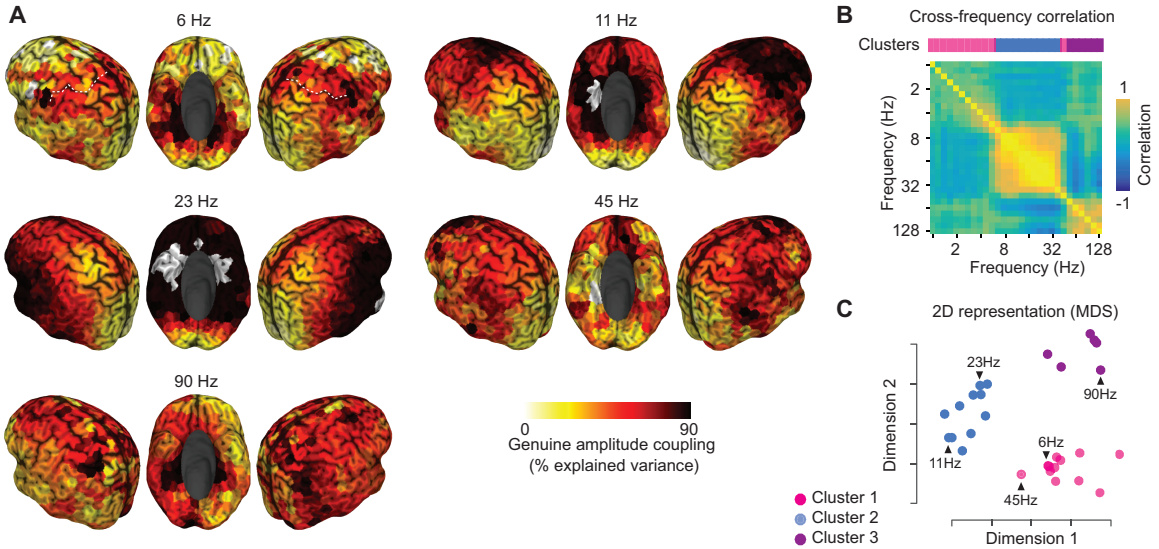

Figure 5. Spatial distribution of genuine amplitude coupling

(A) Spectrally and spatially resolved portion of variance in the measured amplitude coupling that cannot be explained by the amplitude-coupling bias and is thus attributed to genuine amplitude coupling (attenuation corrected). The color scale indicates the amount of genuine variance, i.e. 1-r^2 of the attenuation corrected correlation between measured and biased amplitude coupling. The white dashed line in the top left panel indicates the central sulcus. (B) Cross-frequency correlation of attenuation corrected correlation patterns. The colored bar on top of the matrix indicates the frequency specific clustering of patterns (Gaussian mixture model with 3 clusters for minimal BIC, see 2.11). (C) 2D multidimensional scaling representation of cortical patterns in (A) based on the Euclidean distance between patterns (see 2.11). Points are colored according to the clustering of patterns.

Thus, we applied a leave-one-out jackknifing procedure and false-discovery rate correction (Benjamini and Hochberg, 1995). Across the entire spectrum, we found that more than 90% of the seed patterns showed significant ($p < 0.05$ corrected) physiological amplitude coupling (Fig. 3B). For frequencies above 5 Hz, this ratio increases to more than 98% with large effect sizes (Fig. 3A, blue line), i.e. a large fraction of variance that cannot be explained by the bias and is thus due to genuine physiological amplitude coupling.

The spatial distribution of these effect sizes had a complex spectral pattern (Fig. 5A). A cluster analysis revealed three major patterns (Fig. 5B and C, lowest BIC for 3 clusters): For frequencies from 7 to 32 Hz strongest physiological amplitude coupling was expressed in frontal and ventral regions, whereas physiological amplitude coupling is particularly strong in more posterior and parietal regions for very high frequencies. Furthermore, physiological amplitude coupling peaks in pericentral areas for the very low frequencies and around 45Hz.

Overall, these results indicate that the measured amplitude coupling is indeed different from the spurious coupling introduced by phase coupling and volume conduction. Furthermore, for most parts of the brain and frequencies physiological amplitude coupling accounts for 70 % and more of the variance in cortical amplitude coupling patterns.

Comparing physiological amplitude coupling with phase coupling networks

Establishing a physiological component in amplitude coupling allowed us to address our second question, i.e. if there are differences between amplitude and phase coupling patterns. Although we can quantify the amount of variance due to physiological amplitude coupling, we cannot directly extract physiological amplitude-coupling patterns. This precludes a direct comparison between physiological amplitude coupling and phase coupling patterns. However, we can indirectly infer differences between these patterns by conceptualizing them as vectors within a high-dimensional space (Fig. 6), in which their co-linearity describes their similarity (correlation). We know that amplitude-coupling bias patterns (AC_{bias}) are a positively weighted average of the phase coupling (PC) and field spread (M) vectors (Fig. 6A).

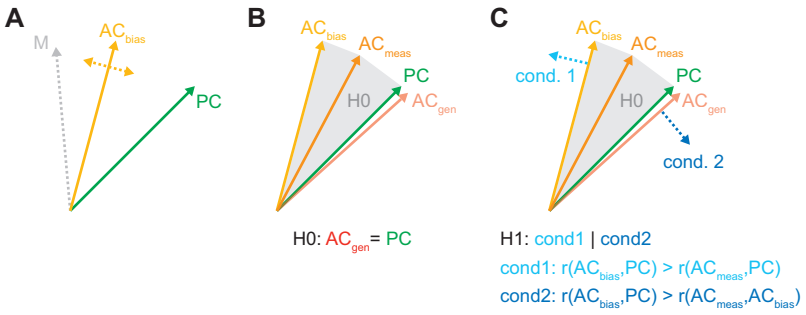

Figure 6. Schematic comparison of phase-coupling and genuine amplitude-coupling patterns

A direct comparison of phase-coupling patterns and genuine amplitude-coupling patterns is not possible, because the genuine part of amplitude-coupling patterns cannot be observed directly. However, different patterns can be inferred by if either one of two critical conditions are met. This is shown here by conceptualizing cortical patterns, which for the present data are 457-dimensional vectors, as two-dimensional vectors with unit length. The co-linearity between vectors corresponds to the correlation of these patterns. (A) The mixing pattern (M) (field spread) and the phase coupling pattern (PC) is empirically measured. The amplitude-coupling bias (AC_{bias}) corresponds to a weighted average of PC and M. (B) The measured amplitude coupling (AC_{meas}) is a weighted average of the genuine physiological amplitude coupling (AC_{gen}) and the bias. Under the Null-hypothesis that genuine amplitude coupling and phase coupling patterns are identical, AC_{meas} is situated in the hyper-area between AC_{bias} and PC. (C) If AC_{meas} is outside the H0-area, we accept the alternative hypothesis that AC_{gen} and PC are different. AC_{gen} is outside the H0-area if either condition 1 (light blue) or condition 2 (dark blue) is met.

Thus, AC_{bias} is situated in the hyper area between PC and M. Under the Null hypothesis, the physiological amplitude coupling pattern (AC_{gen}) is the same as the phase-coupling pattern (Fig. 6B). As the measured amplitude coupling pattern (AC_{meas}) is a summation of the bias and the physiological amplitude coupling patterns (Palva et al., 2018), under the Null hypothesis, AC_{meas} is situated in the area between the bias and phase coupling (Fig. 6B). Hence, if the measured amplitude coupling is outside that area we accept the alternative hypothesis that physiological amplitude coupling and phase coupling are not identical (Fig. 6C).

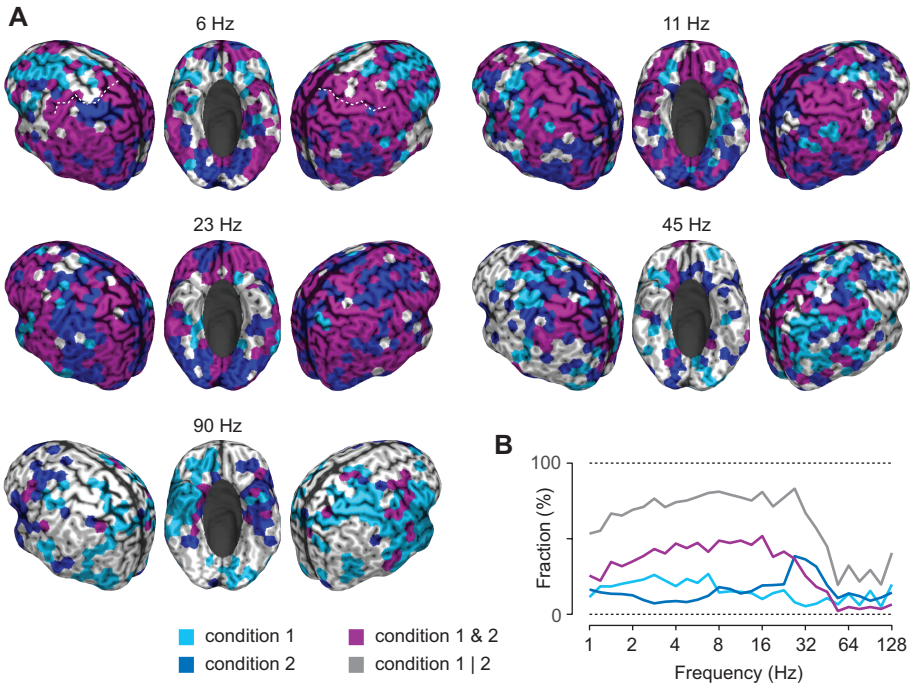

Figure 7. Differences between genuine amplitude-coupling and phase-coupling patterns
(A) Cortical distribution of regions that show significant differences between genuine amplitude-coupling and phase-coupling patterns by fulfilling either condition 1 (light blue), condition 2 (dark blue) or both (purple). (B) Fraction of cortical regions that show significant differences between genuine amplitude-coupling and phase-coupling patterns. Same color-scheme as in (A). In addition, the gray line indicates the fraction of regions that fulfill either condition 1 or 2 (see 2.10 for details).

AC_{meas} is outside the Null-hypothesis area either if the AC_{bias}-PC correlation is larger than the AC_{meas}-PC correlation (condition 1) or if the AC_{bias}-PC correlation is larger than the AC_{meas}-AC_{bias} (condition 2) (Fig. 6C). To test these conditions, we computed attenuation corrected correlations between AC_{bias}-PC, AC_{meas}-PC and AC_{meas}-AC_{bias}, and applied leave-one-out Jackknifing to test for significant differences (FDR-corrected).

We found that for large parts of the brain and for all frequencies there were significant differences between cortical phase- and amplitude-coupling patterns (Fig. 7). For

frequencies below and above 45 Hz, amplitude and phase coupling differed for more than about 80% and 40% of the cortex, respectively (Fig. 7B).

These results establish a clear distinction between amplitude- and phase coupling on the network level. The dissociation between conditions 1 and 2 provided further insights into the nature of this distinction. In the frequency range from 8 to 40 Hz, condition 2 was met more often than condition 1 (Fig. 7A and B).

For condition 2, the physiological amplitude coupling vector (AC_{phy}) is further away from the field-spread vector (M) than the phase coupling vector (PC). Thus, in particular in this frequency range, more complex amplitude coupling patterns may predominate. Overall, the spatial distribution of coupling-mode differences covered most of the cortex for lower frequencies and tapered off above 45 Hz to parietal and temporal areas mainly comprising condition 1 (Fig. 7A). Furthermore, at 6 Hz, we observed an anterior to posterior gradient from condition 1 to condition 2.

Discussion

Our results provide, to our knowledge, the first systematic comparison of cortical phase- and amplitude-coupling patterns in the human brain. We found differences between both coupling modes that are widely distributed over frequencies and the entire cortex. Furthermore, by combining empirical measurements and simulations we ruled out that these differences are caused by methodological biases, but instead reflect a genuine neuronal dissociation. The observed differences suggest that cortical phase- and amplitude-coupling patterns are not fully explained by one common underlying mechanism. Instead, our results suggest distinct neural mechanisms underlying both coupling modes in the human brain. Furthermore, our results highlight and clarify the compound nature of amplitude coupling measures applied to orthogonalized signals.

Discounting confounding factors

Our analyses discounted two critical factors that confound the estimation of neuronal coupling patterns and their comparison. First, we employed amplitude correlations of orthogonalized signals (Hipp et al., 2012) and the weighted phase-lag index (Vinck et al., 2011). Using these coupling measures ensured that the measured coupling did not reflect spurious coupling due to field-spread. Second, for the comparison between coupling modes, we employed attenuation correction of correlations (Spearman, 1904). This approach allows correcting for the attenuation of measured correlation caused by sub-optimal measurement reliability. Attenuation correction of correlations is a powerful analytical approach that has been successfully employed before to compare MEG with fMRI (Hipp and Siegel, 2015) and MEG with EEG (Siems et al., 2016). Importantly, reliability in the present study refers to the stability of coupling patterns across subjects, which effectively takes into account all sources of variance across subjects, including measurement and finite-sampling noise, noise caused by neural activity not of interest, and inter-subject variability. The employed approach corrects for all these sources of variance, which attenuate measured correlations and may thus induce spurious spectral and spatial specificity.

Indeed, our results indicate that the raw correlation between the measured amplitude coupling patterns and the bias is strongly affected by measurement reliability. Attenuation correction suggests that the peaked raw correlation around 16 Hz merely reflects the strength of intrinsic cortical rhythms around this frequency, rather than a strong genuine relation of the underlying amplitude- and bias patterns. The same arguments hold for the comparison between amplitude- and phase coupling.

Phase-coupling sensitivity of orthogonalized amplitude correlation

Our results provide a critical reassessment of well-established amplitude-coupling measures of orthogonalized signals (Brookes et al., 2012; Hipp et al., 2012). It has recently been pointed out that these measures are, in the presence of field-spread, sensitive to phase coupling with non-zero phase lag (Palva et al., 2018). Here, we combined the simulation approach put forward by Palva and colleagues (2018) with empirical measurements to systematically evaluate the sensitivity of these measures to phase coupling across the human cortex.

The extent to which phase coupling can bias amplitude coupling measures critically depends on the amount of field-spread. In agreement with this notion, we found that in particular short distance connections show biased amplitude coupling (Fig. 2). On a brain wide scale, this appears as a stereotypical pattern of connectivity decreasing with distance from the seed regions, independent of seed location or frequency.

Determining physiological amplitude coupling

The bias of amplitude coupling measures left open the possibility that the described amplitude coupling patterns (Brookes et al., 2012; Hipp et al., 2012) merely reflect phase coupling in combination with field spread. Our results provide several lines of evidence against this hypothesis.

First, amplitude correlation bias showed a stereotypical pattern of connectivity decreasing with distance, whereas the measured amplitude patterns showed complex and multimodal distributions (Fig. 2). The distance-resolved comparison further supports the notion of higher than expected complexity in measured amplitude coupling patterns (Fig. 4). Second, the between subject reliability of coupling patterns clearly dissociated measured and biased amplitude coupling (Fig. 3C and D). Third, for most cortical regions and frequencies, the correlation of biased and measured amplitude coupling was

significantly smaller than 1 (Fig. 3B). On average, only 30 % of the variance in amplitude coupling patterns could be explained by the bias (only 10% for long connections, Fig. 4B). Finally, the correlation of the bias and measured amplitude coupling showed a frequency specific cortical pattern (Fig. 5), which is not expected by a mere measurement bias.

In summary, our results show that the amplitude correlation of orthogonalized signals is indeed a compound measure of connectivity, that, in particular for small distances, also reflects phase-coupling. Nevertheless, our results indicate, that the observed amplitude coupling patterns are to a large extent driven by genuine physiological amplitude coupling.

Relation between phase- and amplitude coupling

Taking into account the amplitude coupling bias, we found wide-spread significant differences between phase- and amplitude coupling across the human brain (Fig. 6). Which factors may cause these differences?

First, different non-linearities between coupling modes may induce differences. The same underlying neuronal interaction or common input may have different effects on both coupling modes, thus reducing their correlation. However, in contrast to our present results this effect should be spectrally and spatially unspecific. Thus, such non-linearities cannot entirely explain our findings.

Second, phase- and amplitude-coupling may be differentially affected by non-neuronal artifacts. A particularly strong artifact for frequencies above about 30 Hz is muscle activity. Even if M/EEG data is preprocessed to minimize muscle artifacts, as done here (Larson-Prior et al., 2013), residual muscle activity is often detectable in frontal and temporal regions (Hipp and Siegel, 2013; Siems et al., 2016). Notably, we found strong differences between phase- and amplitude coupling at very high frequencies in these

regions (Fig. 7A). This suggests that the two coupling modes may be differentially susceptible to muscle activity. Indeed, specifically the reliability of phase coupling increased at high frequencies (Fig. 3E), which may indicate stronger susceptibility to muscle artifacts for this coupling mode.

Finally, distinct neuronal mechanisms may underlie both coupling modes. For example, neuromodulatory effects may co-modulate the strength of rhythms in different brain regions. Or, as recently proposed, slow fluctuations of extracellular potassium concentrations and structural connectivity may drive long-range power co-fluctuations (Krishnan et al., 2018). These mechanisms may induce amplitude coupling on a slow temporal scale without causing phase coupling on a fast temporal scale.

Despite the observed significant differences between coupling modes our results are also compatible with similarities between their cortical patterns (compare Fig. 2). Such similarities may result from one or more common underlying neural mechanism. For example, mere synaptic interactions between neuronal populations may induce both, coupling of phases and amplitudes of these neuronal populations. Similarly, common input to neuronal populations will co-modulate and thus couple both, phases and amplitudes (Tewarie et al., 2018). Alternatively, also causal relation between both coupling modes may result in correlations. For example, phase coupling may enhance neuronal interactions and thus enhance amplitude coupling (von Nicolai et al., 2014).

Functional role of coupling modes

Phase-coupling of neuronal population may regulate their interactions by aligning rhythmic excitability fluctuations and rhythmic inputs (Fries, 2015). Similarly, amplitude-coupling may modulate interactions by temporally aligning processing associated with low or high oscillatory amplitudes across brain regions (Siegel et al., 2012; von Nicolai et al., 2014). While the observed differences between coupling modes may reflect such

functional roles, the present results hold independent from such potential functions. In fact, even if phase- or amplitude coupling merely reflect neural interactions without a causal mechanistic role, our results show that these coupling modes provide partially dissociated and thus non-redundant spectral fingerprints of these neuronal interactions. This suggests that both coupling modes provide complimentary information on large-scale neuronal interactions during cognitive processes and on their alteration in neuropsychiatric diseases.

Future directions

Our results provide a critical first step to unravel the relationship between neuronal phase- and amplitude-coupling. Further invasive studies are needed to investigate this relationship and the underlying mechanisms on the cellular and circuit level, as well as to link the present results to spiking activity of individual neurons. Also, investigation of cross-frequency relationships, i.e. between phase- and amplitude-coupling across different frequencies (Brookes et al., 2016; Diekelmann and Born, 2010; Mandke et al., 2018; Schroeder and Lakatos, 2009; Tewarie et al., 2016; von Nicolai et al., 2014) and the application of directed interaction measures (Hillebrand et al., 2016; Lobier et al., 2014; Vinck et al., 2015) may allow to identify generic links between coupling modes.

Methods and Materials

Subjects and dataset

We analyzed resting-state MEG measurements from 95 subjects included in the publicly available human connectome project (HCP) S900 release. Participants were healthy adults in the age range between 22-35 ($n_{22\text{-}25}$ = 18, $n_{26\text{-}30}$ = 40, $n_{31\text{-}35}$ = 37). The sample included 45 females. The resting-state measurements included three six-minute blocks with short breaks in between measurements. Data were recorded with a whole-head Magnes 3600 scanner (4D Neuroimaging, San Diego, CA, USA) situated in a magnetically shielded room (for further details see: Larson-Prior et al., 2013). Additionally, the subjects were scanned on a Siemens 3T Skyra to acquire structural T1-weighted magnetic resonance images (MRI) with 0.7mm isotropic resolution (Van Essen et al., 2013).

Data preprocessing

We used the preprocessed data as it is provided by the HCP pipeline (Larson-Prior et al., 2013). This includes removal of noisy and bad channels, bad data segments and physiological artifacts by the iterative application of temporal and spatial independent component analysis (ICA) (Larson-Prior et al., 2013; Mantini et al., 2011).

Physical forward model and source modeling

MEG sensors were aligned to the individual anatomy using FieldTrip (Oostenveld et al., 2010). We segmented the individual T1-weighted images and generated a single shell head model to compute the physical forward model (Nolte, 2003). We computed the forward model for 457 equally spaced (~1.2cm distance) source points spanning the cortex at 0.7 cm depth below the pial surface (Hipp and Siegel, 2015). This source shell was generated in MNI-space and non-linearly transformed to individual headspace.

Source coordinates, head model and MEG channels were co-registered on the basis of three head localization coils.

The sensor-level MEG data was projected to source space using linear beamforming (Gross et al., 2001; Van Veen et al., 1997). This spatial filtering approach reconstructs activity of the sources of interest with unit gain while maximally suppressing contributions from other sources.

Coordinates for the seed-based connectivity analyses were adopted from Hipp et al. (2012). For every seed, the source location of the 457 shell positions with minimum Euclidean distance from the seed coordinates was chosen: left auditory cortex (lAC) [-54, -22, 10]; left somatosensory cortex (lSSC) [42, -26, 54]; medial prefrontal cortex (MPFC) [-3, 39, -2] (all MNI coordinates).

Spectral analysis

Time-frequency estimates of the time-domain MEG signal were generated using Morlet's wavelets (Goupillaud et al., 1984). The bandwidth of the wavelets was set to 0.5 octaves (1 spectral standard deviation) with a temporal step-size of half the temporal standard deviation. We derived spectral estimates for frequencies from 1 to 128 Hz in quarter octave steps.

Coupling measures

We estimated amplitude coupling using amplitude envelope correlations of orthogonalized signals (Hipp et al., 2012). We correlated (Pearson's r) the log-transformed power envelopes pairwise between brain areas. Volume conduction effect were discounted by orthogonalizing the two complex signals at each point in time before correlation (Brookes et al., 2012; Hipp et al., 2012).

As a measure of phase coupling we adapted the weighted phase lag index (wPLI; Vinck et al., 2011). The wPLI takes only the imaginary part of the cross-spectrum into account

and normalizes it with the maximum imaginary contribution within the time series. The imaginary part of the cross-spectrum is insensitive to volume conduction since it has no contribution from zero phase lagged parts of the signal (Nolte et al., 2004; Vinck et al., 2011). We computed both coupling measures for the full adjacency matrices for all subjects and frequency bands.

Data simulation

We employed a simulation approach put forward by Palva and colleagues (2018). For every connection, frequency and subject we generated two signals x and y as complex representations:

$$x = A_x(t)e^{ip_x(t)} + mA_y(t)e^{i(p_y(t)+s_{x,y})}$$

$$y = A_y(t)e^{i(p_y(t)+s_{x,y})} + mA_x(t)e^{ip_x(t)}$$

$A(t)$ and $p(t)$ are vectors representing the amplitude and the phase of the sources, respectively. In analogy to volume conduction the source data is linearly mixed by the parameter m. This value is determined from the empirical data as the sum of the diagonal elements from the multiplication of the filter matrix $F_{x,f}$ with the leadfield L_y. The mixing parameter can be determined in both direction, i.e. x to y and y to x, and we chose the mean of these two values for any given connection between x and y. Additionally, $s_{x,y}$ refers to the constant phase shift introduced between the sources. We chose the worst case scenario and set the phase shift to 90 degrees (Palva et al., 2018). The amplitude $A(t)$ vectors were determined as follows:

$$A_x(t) = |F\big(n_1(t) + c_A n_2(t)\big)|$$

$$A_y(t) = |F\big(n_2(t) + c_A n_1(t)\big)|$$

$n_1(t)$ and $n_2(t)$ refer to vectors of random numbers with data length of 300 seconds with a sampling frequency of 400 Hz approximately matching the original data length (Larson-Prior et al., 2013) and || refers to the modulus. c_A denotes the ground truth

amplitude coupling between the sources x and y and was set to 0. The function F is the complex wavelet transformation of the vectors at the frequency of interest. The wavelet transformation parameter matched our analysis of the empirical data (see above). Analogously, we generated the phase $p(t)$ vectors:

$$p_x(t) = |F\left(n_3(t) + c_p n_4(t)\right)|$$

$$p_y(t) = |F\left(n_4(t) + c_p n_3(t)\right)|$$

$n_3(t)$ and $n_4(t)$ are again 300 s vectors of random numbers at a sampling frequency of 400 Hz. All 4 n vectors are drawn anew for every connection. c_p denotes the ground truth phase coupling in our simulation and is set to the empirical weighted phase lag index for every connection, frequency and subject.

Finally, we computed the amplitude coupling of the orthogonalized signals x and y (see above).

Reliability estimation

To compare the reliability, i.e. reproducibility, of each functional connectivity measure, we correlated the seed patterns within (Fig. 3) and between subjects (Fig. 3, 4 & 7). We correlated each column in the adjacency matrices pairwise, either between subjects (between subjects reliability) or between runs (within subject reliability). For the between-subject comparison, we further averaged the adjacency matrices acquired in the three runs of each subject before correlating between subjects. For further analyses, we averaged the reliabilities across comparisons and statistically tested against zero (one-sided t-test, FDR correction).

Intermeasure correlation and attenuation correction

We correlated the cortical bias, amplitude and phase coupling patters (columns of adjacency matrix) pairwise for each seed between subjects. This spectrally and spatially

resolved the pairwise similarity between measures. However, this estimate of pattern similarity is biased by the reliability of patterns within each measure, i.e. their signal-to-noise ratio (Hipp and Siegel, 2015; Siems et al., 2016). This effect decreases the correlation between measures depending on the signal-to-noise ratio. We corrected this bias by applying the correction of attenuated correlations according to (Spearman 1904). Hereby, we estimated the signal-to-noise ratio as the reliability within each measure and divided the correlation between measures by the pooled within-measure reliability.

$$r_{corr} = \frac{r_{measure1\backslash measure2}}{\sqrt{r_{measure1}}\sqrt{r_{measure2}}}$$

Statistical testing of attenuation corrected correlations

A perfect attenuation corrected correlation (r_{corr} = 1) indicates that two cortical patterns are identical if there was perfect reliability. A value smaller than 1 indicates that there is a difference between the two patterns that cannot only be explained by reduced reliability. For statistical testing, we applied leave-one-out Jackknifing and computed pseudo-values to generate a subject specific distribution of attenuation corrected values. This procedure produces one distribution per source and frequency. Given these distributions and the characteristics of attenuation corrected correlations (Fig. S1) we performed one-sided t-tests against 1. We corrected the resulting p-values with false-discovery rate correction within each frequency (Benjamini and Hochberg, 1995).

Unfortunately, statistical testing re-introduces signal-to-noise ratio effects into the analysis. The mean pseudo-values are still free from this effect but the subject-specific variability is affected. Hence, the statistical power is influenced by the signal-to-noise ratio. This caveat needs to be taken into account when interpreting the statistical significance.

Quantifying the difference between physiological amplitude coupling and phase coupling

It is impossible to directly assess the physiological amplitude coupling, which prevents a direct comparison between physiological amplitude coupling and phase coupling patterns. Thus, we conceptualized these patterns as vectors in a high-dimensional space (Fig. 6) where vector co-linearity describes how strongly patterns are correlated. Under the Null hypothesis the physiological amplitude coupling (AC_{phy}) is the same as the phase coupling pattern (AC_{gen}=PC; Fig. 6B). The measured amplitude coupling (AC_{meas}) is a summation of the bias and the physiological amplitude coupling (Palva et al., 2018) and, under the Null hypothesis, is comprised in the area between the bias (AC_{bias}) and phase coupling. We can quantify the alternative hypothesis using the co-linearity of these vectors, i.e. correlation: under condition 1 the AC_{bias}-PC correlation is larger than the AC_{meas}-PC correlation. Under condition 2 the AC_{bias}-PC correlation is larger than the AC_{meas}-AC_{bias} correlation (Fig. 6C). If one of the two conditions is fulfilled, we reject the Null hypothesis. We used the attenuation corrected correlations between AC_{bias}-PC, AC_{meas}-PC and AC_{meas}-AC_{bias} to test the hypothesis. We applied leave-one-out Jackknifing to compute three pseudo-value distributions per source and frequency and performed one-sided paired t-tests to identify sources that fulfill at least one of the two conditions:

$$condition\ 1\text{:}\ \mathrm{r}_{\mathrm{AC_{bias}},\mathrm{PC}} - \mathrm{r}_{\mathrm{AC_{meas}},\mathrm{PC}} > 0$$

$$condition\ 2\text{:}\ \mathrm{r}_{\mathrm{AC_{bias}},\mathrm{PC}} - \mathrm{r}_{\mathrm{AC_{meas}},\mathrm{AC}_{bias}} > 0$$

$r_{ACbias,PC}$, $r_{ACmeas,PC}$ and $r_{ACmeas,ACbias}$ refer to the pseudo-value distributions of each source and frequency. We use FDR-correction ($p < 0.025$ corrected) within each frequency.

Clustering of attenuation corrected patterns

To assess a possible frequency specificity of attenuation corrected correlation patterns between measured and biased amplitude coupling, we clustered these patterns using Gaussian mixed modeling (compare Fig. 5B. We clustered the frequency specific patterns using 1 to 8 Gaussians in each model and assessed the trade off between explanatory power and complexity of each model with the Bayesian information criterion (BIC). This analysis yielded an optimal model complexity of 3.

We visualized the clustering results in two ways: First, a cross-frequency correlation of patterns between all frequency pairs (Fig. 5C). This yielded a frequency-by-frequency correlation between patterns. Second, we used multidimensional scaling to represent the patterns in two dimensions (Fig. 5D). As distance matrix for the MDS algorithm we computed the Euclidean distance pairwise between all patterns.

Author Contributions

Both authors conceived the study, wrote and revised the paper. M.S.1 performed the data analysis.

Acknowledgments

The authors declare no conflict of interest. This study was supported by the European Research Council (ERC StG335880) and the Centre for Integrative Neuroscience (DFG, EXC 307). We further thank Constantin von Nicolai, Nima Noury and Andrea Ibarra Chaoul for help with the manuscript and useful discussions. We thank Joerg Hipp for valuable ideas regarding the data analysis.

References

Akam, T., Kullmann, D.M., 2014. Oscillatory multiplexing of population codes for selective communication in the mammalian brain. Nat. Rev. Neurosci. 15, 111–122. https://doi.org/10.1038/nrn3668

Benjamini, Y., Hochberg, Y., 1995. Controlling the False Discovery Rate: A Practical and Powerful Approach to Multiple Testing. J. R. Stat. Soc. Ser. B Methodol. 57, 289–300.

Bergholm, F., Adler, J., Parmryd, I., 2010. Analysis of bias in the apparent correlation coefficient between image pairs corrupted by severe noise. J. Math. Imaging Vis. 37, 204–219.

Bosman, C.A., Schoffelen, J.-M., Brunet, N., Oostenveld, R., Bastos, A.M., Womelsdorf, T., Rubehn, B., Stieglitz, T., De Weerd, P., Fries, P., 2012. Attentional Stimulus Selection through Selective Synchronization between Monkey Visual Areas. Neuron 75, 875–888. https://doi.org/10.1016/j.neuron.2012.06.037

Brookes, M.J., Tewarie, P.K., Hunt, B.A.E., Robson, S.E., Gascoyne, L.E., Liddle, E.B., Liddle, P.F., Morris, P.G., 2016. A multi-layer network approach to MEG connectivity analysis. NeuroImage 132, 425–438. https://doi.org/10.1016/j.neuroimage.2016.02.045

Brookes, M.J., Woolrich, M., Luckhoo, H., Price, D., Hale, J.R., Stephenson, M.C., Barnes, G.R., Smith, S.M., Morris, P.G., 2011. Investigating the electrophysiological basis of resting state networks using magnetoencephalography. Proc. Natl. Acad. Sci. U. S. A. 108, 16783–16788. https://doi.org/10.1073/pnas.1112685108

Brookes, M.J., Woolrich, M.W., Barnes, G.R., 2012. Measuring functional connectivity in MEG: a multivariate approach insensitive to linear source leakage. NeuroImage 63,

910–920. https://doi.org/10.1016/j.neuroimage.2012.03.048

Bruns, A., Eckhorn, R., Jokeit, H., Ebner, A., 2000. Amplitude envelope correlation detects coupling among incoherent brain signals. Neuroreport 11, 1509–1514.

Burns, S.P., Santaniello, S., Yaffe, R.B., Jouny, C.C., Crone, N.E., Bergey, G.K., Anderson, W.S., Sarma, S.V., 2014. Network dynamics of the brain and influence of the epileptic seizure onset zone. Proc. Natl. Acad. Sci. 111, E5321–E5330. https://doi.org/10.1073/pnas.1401752111

Buschman, T.J., Denovellis, E.L., Diogo, C., Bullock, D., Miller, E.K., 2012. Synchronous oscillatory neural ensembles for rules in the prefrontal cortex. Neuron 76, 838–846. https://doi.org/10.1016/j.neuron.2012.09.029

Buschman, T.J., Miller, E.K., 2007. Top-down versus bottom-up control of attention in the prefrontal and posterior parietal cortices. Science 315, 1860–2.

Cetin, M.S., Houck, J.M., Rashid, B., Agacoglu, O., Stephen, J.M., Sui, J., Canive, J., Mayer, A., Aine, C., Bustillo, J.R., Calhoun, V.D., 2016. Multimodal Classification of Schizophrenia Patients with MEG and fMRI Data Using Static and Dynamic Connectivity Measures. Front. Neurosci. 10. https://doi.org/10.3389/fnins.2016.00466

Colclough, G.L., Woolrich, M.W., Tewarie, P.K., Brookes, M.J., Quinn, A.J., Smith, S.M., 2016. How reliable are MEG resting-state connectivity metrics? NeuroImage 138, 284–293. https://doi.org/10.1016/j.neuroimage.2016.05.070

Cover, K.S., Vrenken, H., Geurts, J.J.G., van Oosten, B.W., Jelles, B., Polman, C.H., Stam, C.J., van Dijk, B.W., 2006. Multiple sclerosis patients show a highly significant decrease in alpha band interhemispheric synchronization measured using MEG. NeuroImage 29, 783–788. https://doi.org/10.1016/j.neuroimage.2005.08.048

Deco, G., Corbetta, M., 2011. The dynamical balance of the brain at rest. Neurosci. Rev. J. Bringing Neurobiol. Neurol. Psychiatry 17, 107–123. https://doi.org/10.1177/1073858409354384

Destexhe, A., Contreras, D., Steriade, M., 1999. Spatiotemporal analysis of local field potentials and unit discharges in cat cerebral cortex during natural wake and sleep states. J. Neurosci. Off. J. Soc. Neurosci. 19, 4595–4608.

Diekelmann, S., Born, J., 2010. The memory function of sleep. Nat. Rev. Neurosci. 11, 114–126. https://doi.org/10.1038/nrn2762

Engel, A.K., Fries, P., Singer, W., 2001. Dynamic predictions: oscillations and synchrony in top-down processing. Nat. Rev. Neurosci. 2, 704–716. https://doi.org/10.1038/35094565

Engel, A.K., Gerloff, C., Hilgetag, C.C., Nolte, G., 2013. Intrinsic coupling modes: multiscale interactions in ongoing brain activity. Neuron 80, 867–886. https://doi.org/10.1016/j.neuron.2013.09.038

Fell, J., Axmacher, N., 2011. The role of phase synchronization in memory processes. Nat Rev Neurosci 12, 105–18. https://doi.org/10.1038/nrn2979

Fornito, A., Zalesky, A., Breakspear, M., 2015. The connectomics of brain disorders. Nat. Rev. Neurosci. 16, 159–172. https://doi.org/10.1038/nrn3901

Fries, P., 2015. Rhythms for Cognition: Communication through Coherence. Neuron 88, 220–235. https://doi.org/10.1016/j.neuron.2015.09.034

Goupillaud, P., Grossmann, A., Morlet, J., 1984. Cycle-octave and related transforms in seismic signal analysis. Geoexploration, Seismic Signal Analysis and Discrimination III 23, 85–102. https://doi.org/10.1016/0016-7142(84)90025-5

Gregoriou, G.G., Gotts, S.J., Zhou, H., Desimone, R., 2009. High-frequency, long-range coupling between prefrontal and visual cortex during attention. Science 324, 1207–10. https://doi.org/10.1126/science.1171402

Gross, J., Kujala, J., Hamalainen, M., Timmermann, L., Schnitzler, A., Salmelin, R., 2001. Dynamic imaging of coherent sources: Studying neural interactions in the human brain. Proc. Natl. Acad. Sci. U. S. A. 98, 694–699. https://doi.org/10.1073/pnas.98.2.694

Hawellek, D.J., Schepers, I.M., Roeder, B., Engel, A.K., Siegel, M., Hipp, J.F., 2013. Altered intrinsic neuronal interactions in the visual cortex of the blind. J. Neurosci. Off. J. Soc. Neurosci. 33, 17072–17080. https://doi.org/10.1523/JNEUROSCI.1625-13.2013

Hillebrand, A., Barnes, G.R., Bosboom, J.L., Berendse, H.W., Stam, C.J., 2012. Frequency-dependent functional connectivity within resting-state networks: an atlas-based MEG beamformer solution. NeuroImage 59, 3909–3921. https://doi.org/10.1016/j.neuroimage.2011.11.005

Hillebrand, A., Tewarie, P., van Dellen, E., Yu, M., Carbo, E.W.S., Douw, L., Gouw, A.A., van Straaten, E.C.W., Stam, C.J., 2016. Direction of information flow in large-scale resting-state networks is frequency-dependent. Proc. Natl. Acad. Sci. U. S. A. 113, 3867–3872. https://doi.org/10.1073/pnas.1515657113

Hipp, J.F., Engel, A.K., Siegel, M., 2011. Oscillatory synchronization in large-scale cortical networks predicts perception. Neuron 69, 387–396. https://doi.org/10.1016/j.neuron.2010.12.027

Hipp, J.F., Hawellek, D.J., Corbetta, M., Siegel, M., Engel, A.K., 2012. Large-scale cortical correlation structure of spontaneous oscillatory activity. Nat. Neurosci. 15,

884–890. https://doi.org/10.1038/nn.3101

Hipp, J.F., Siegel, M., 2015. BOLD fMRI Correlation Reflects Frequency-Specific Neuronal Correlation. Curr. Biol. CB 25, 1368–1374. https://doi.org/10.1016/j.cub.2015.03.049

Hipp, J.F., Siegel, M., 2013. Dissociating neuronal gamma-band activity from cranial and ocular muscle activity in EEG. Front. Hum. Neurosci. 7, 338. https://doi.org/10.3389/fnhum.2013.00338

Jahnke, S., Memmesheimer, R.-M., Timme, M., 2014. Oscillation-induced signal transmission and gating in neural circuits. PLoS Comput. Biol. 10, e1003940. https://doi.org/10.1371/journal.pcbi.1003940

Jensen, O., Mazaheri, A., 2010. Shaping functional architecture by oscillatory alpha activity: gating by inhibition. Front. Hum. Neurosci. 4, 186. https://doi.org/10.3389/fnhum.2010.00186

Kitzbichler, M.G., Khan, S., Ganesan, S., Vangel, M.G., Herbert, M.R., Hämäläinen, M.S., Kenet, T., 2015. Altered development and multifaceted band-specific abnormalities of resting state networks in autism. Biol. Psychiatry 77, 794–804. https://doi.org/10.1016/j.biopsych.2014.05.012

Koelewijn, L., Bompas, A., Tales, A., Brookes, M.J., Muthukumaraswamy, S.D., Bayer, A., Singh, K.D., 2017. Alzheimer's disease disrupts alpha and beta-band resting-state oscillatory network connectivity. Clin. Neurophysiol. https://doi.org/10.1016/j.clinph.2017.04.018

Krishnan, G.P., González, O.C., Bazhenov, M., 2018. Origin of slow spontaneous resting-state neuronal fluctuations in brain networks. Proc. Natl. Acad. Sci. U. S. A. https://doi.org/10.1073/pnas.1715841115

Larson-Prior, L.J., Oostenveld, R., Della Penna, S., Michalareas, G., Prior, F., Babajani-Feremi, A., Schoffelen, J.-M., Marzetti, L., de Pasquale, F., Di Pompeo, F., Stout, J., Woolrich, M., Luo, Q., Bucholz, R., Fries, P., Pizzella, V., Romani, G.L., Corbetta, M., Snyder, A.Z., 2013. Adding dynamics to the Human Connectome Project with MEG. NeuroImage, Mapping the Connectome 80, 190–201. https://doi.org/10.1016/j.neuroimage.2013.05.056

Larson-Prior, L.J., Power, J.D., Vincent, J.L., Nolan, T.S., Coalson, R.S., Zempel, J., Snyder, A.Z., Schlaggar, B.L., Raichle, M.E., Petersen, S.E., 2011. Modulation of the brain's functional network architecture in the transition from wake to sleep. Prog. Brain Res. 193, 277–294. https://doi.org/10.1016/B978-0-444-53839-0.00018-1

Leopold, D.A., Murayama, Y., Logothetis, N.K., 2003. Very slow activity fluctuations in monkey visual cortex: implications for functional brain imaging. Cereb. Cortex N. Y. N 1991 13, 422–433.

Lobier, M., Siebenhühner, F., Palva, S., Palva, J.M., 2014. Phase transfer entropy: a novel phase-based measure for directed connectivity in networks coupled by oscillatory interactions. NeuroImage 85 Pt 2, 853–872. https://doi.org/10.1016/j.neuroimage.2013.08.056

Lopes da Silva, F., 2013. EEG and MEG: relevance to neuroscience. Neuron 80, 1112–1128. https://doi.org/10.1016/j.neuron.2013.10.017

Maestú, F., Peña, J.-M., Garcés, P., González, S., Bajo, R., Bagic, A., Cuesta, P., Funke, M., Mäkelä, J.P., Menasalvas, E., Nakamura, A., Parkkonen, L., López, M.E., del Pozo, F., Sudre, G., Zamrini, E., Pekkonen, E., Henson, R.N., Becker, J.T., 2015. A multicenter study of the early detection of synaptic dysfunction in Mild Cognitive Impairment using Magnetoencephalography-derived functional

connectivity. NeuroImage Clin. 9, 103–109. https://doi.org/10.1016/j.nicl.2015.07.011

Mandke, K., Meier, J., Brookes, M.J., O'Dea, R.D., Van Mieghem, P., Stam, C.J., Hillebrand, A., Tewarie, P., 2018. Comparing multilayer brain networks between groups: Introducing graph metrics and recommendations. NeuroImage 166, 371–384. https://doi.org/10.1016/j.neuroimage.2017.11.016

Mantini, D., Penna, S.D., Marzetti, L., de Pasquale, F., Pizzella, V., Corbetta, M., Romani, G.L., 2011. A Signal-Processing Pipeline for Magnetoencephalography Resting-State Networks. Brain Connect. 1, 49–59. https://doi.org/10.1089/brain.2011.0001

Mantini, D., Perrucci, M.G., Del Gratta, C., Romani, G.L., Corbetta, M., 2007. Electrophysiological signatures of resting state networks in the human brain. Proc. Natl. Acad. Sci. U. S. A. 104, 13170–13175. https://doi.org/10.1073/pnas.0700668104

Maran, M., Grent-'t-Jong, T., Uhlhaas, P.J., 2016. Electrophysiological insights into connectivity anomalies in schizophrenia: a systematic review. Neuropsychiatr. Electrophysiol. 2, 6. https://doi.org/10.1186/s40810-016-0020-5

Mehrkanoon, S., Breakspear, M., Britz, J., Boonstra, T.W., 2014. Intrinsic coupling modes in source-reconstructed electroencephalography. Brain Connect. 4, 812–825. https://doi.org/10.1089/brain.2014.0280

Nir, Y., Mukamel, R., Dinstein, I., Privman, E., Harel, M., Fisch, L., Gelbard-Sagiv, H., Kipervasser, S., Andelman, F., Neufeld, M.Y., Kramer, U., Arieli, A., Fried, I., Malach, R., 2008. Interhemispheric correlations of slow spontaneous neuronal fluctuations revealed in human sensory cortex. Nat. Neurosci. 11, 1100–1108.

Nolte, G., 2003. The magnetic lead field theorem in the quasi-static approximation and its use for magnetoencephalography forward calculation in realistic volume conductors. Phys. Med. Biol. 48, 3637. https://doi.org/10.1088/0031-9155/48/22/002

Nolte, G., Bai, O., Wheaton, L., Mari, Z., Vorbach, S., Hallett, M., 2004. Identifying true brain interaction from EEG data using the imaginary part of coherency. Clin. Neurophysiol. Off. J. Int. Fed. Clin. Neurophysiol. 115, 2292–2307. https://doi.org/10.1016/j.clinph.2004.04.029

O'Neill, G.C., Barratt, E.L., Hunt, B.A.E., Tewarie, P.K., Brookes, M.J., 2015. Measuring electrophysiological connectivity by power envelope correlation: a technical review on MEG methods. Phys. Med. Biol. 60, R271-295. https://doi.org/10.1088/0031-9155/60/21/R271

Oostenveld, R., Fries, P., Maris, E., Schoffelen, J.-M., 2010. FieldTrip: Open Source Software for Advanced Analysis of MEG, EEG, and Invasive Electrophysiological Data. Comput. Intell. Neurosci. 2011, e156869. https://doi.org/10.1155/2011/156869

Oswal, A., Beudel, M., Zrinzo, L., Limousin, P., Hariz, M., Foltynie, T., Litvak, V., Brown, P., 2016. Deep brain stimulation modulates synchrony within spatially and spectrally distinct resting state networks in Parkinson's disease. Brain 139, 1482–1496. https://doi.org/10.1093/brain/aww048

Palva, J.M., Monto, S., Kulashekhar, S., Palva, S., 2010. Neuronal synchrony reveals working memory networks and predicts individual memory capacity. Proc Natl Acad Sci U A 107, 7580–5. https://doi.org/10.1073/pnas.0913113107

Palva, J.M., Wang, S.H., Palva, S., Zhigalov, A., Monto, S., Brookes, M.J., Schoffelen, J.-M., Jerbi, K., 2018. Ghost interactions in MEG/EEG source space: A note of caution on inter-areal coupling measures. NeuroImage 173, 632–643.

https://doi.org/10.1016/j.neuroimage.2018.02.032

Schoonheim, M.M., Geurts, J.J.G., Landi, D., Douw, L., van der Meer, M.L., Vrenken, H., Polman, C.H., Barkhof, F., Stam, C.J., 2013. Functional connectivity changes in multiple sclerosis patients: A graph analytical study of MEG resting state data. Hum. Brain Mapp. 34, 52–61. https://doi.org/10.1002/hbm.21424

Schroeder, C.E., Lakatos, P., 2009. Low-frequency neuronal oscillations as instruments of sensory selection. Trends Neurosci. 32, 9–18. https://doi.org/10.1016/j.tins.2008.09.012

Siegel, M., Donner, T.H., Engel, A.K., 2012. Spectral fingerprints of large-scale neuronal interactions. Nat. Rev. Neurosci. 13, 121–134. https://doi.org/10.1038/nrn3137

Siegel, M., Donner, T.H., Oostenveld, R., Fries, P., Engel, A.K., 2008. Neuronal synchronization along the dorsal visual pathway reflects the focus of spatial attention. Neuron 60, 709–719. https://doi.org/10.1016/j.neuron.2008.09.010

Siems, M., Pape, A.-A., Hipp, J.F., Siegel, M., 2016. Measuring the cortical correlation structure of spontaneous oscillatory activity with EEG and MEG. NeuroImage 129, 345–355. https://doi.org/10.1016/j.neuroimage.2016.01.055

Singer, W., 2013. Cortical dynamics revisited. Trends Cogn. Sci., Special Issue: The Connectome 17, 616–626. https://doi.org/10.1016/j.tics.2013.09.006

Singer, W., 1999. Neuronal Synchrony: A Versatile Code for the Definition of Relations? Neuron 24, 49–65. https://doi.org/10.1016/S0896-6273(00)80821-1

Spearman, C., 1904. The proof and measurement of association between two things. Am. J. Psychol. 15, 72–101.

Stam, C.J., 2014. Modern network science of neurological disorders. Nat. Rev. Neurosci.

15, 683–695. https://doi.org/10.1038/nrn3801

Tewarie, P., Hillebrand, A., Schoonheim, M.M., van Dijk, B.W., Geurts, J.J.G., Barkhof, F., Polman, C.H., Stam, C.J., 2014. Functional brain network analysis using minimum spanning trees in Multiple Sclerosis: An MEG source-space study. NeuroImage 88, 308–318. https://doi.org/10.1016/j.neuroimage.2013.10.022

Tewarie, P., Hillebrand, A., van Dijk, B.W., Stam, C.J., O'Neill, G.C., Van Mieghem, P., Meier, J.M., Woolrich, M.W., Morris, P.G., Brookes, M.J., 2016. Integrating cross-frequency and within band functional networks in resting-state MEG: A multi-layer network approach. NeuroImage 142, 324–336. https://doi.org/10.1016/j.neuroimage.2016.07.057

Tewarie, P., Hunt, B.A.E., O'Neill, G.C., Byrne, A., Aquino, K., Bauer, M., Mullinger, K.J., Coombes, S., Brookes, M.J., 2018. Relationships Between Neuronal Oscillatory Amplitude and Dynamic Functional Connectivity. Cereb. Cortex N. Y. N 1991. https://doi.org/10.1093/cercor/bhy136

Uhlhaas, P.J., Singer, W., 2012. Neuronal dynamics and neuropsychiatric disorders: toward a translational paradigm for dysfunctional large-scale networks. Neuron 75, 963–80. https://doi.org/10.1016/j.neuron.2012.09.004

van Dellen, E., Douw, L., Hillebrand, A., de Witt Hamer, P.C., Baayen, J.C., Heimans, J.J., Reijneveld, J.C., Stam, C.J., 2014. Epilepsy surgery outcome and functional network alterations in longitudinal MEG: A minimum spanning tree analysis. NeuroImage 86, 354–363. https://doi.org/10.1016/j.neuroimage.2013.10.010

Van Essen, D.C., Smith, S.M., Barch, D.M., Behrens, T.E.J., Yacoub, E., Ugurbil, K., 2013. The WU-Minn Human Connectome Project: An overview. NeuroImage, Mapping the Connectome 80, 62–79.

https://doi.org/10.1016/j.neuroimage.2013.05.041

Van Veen, B.D., van Drongelen, W., Yuchtman, M., Suzuki, A., 1997. Localization of brain electrical activity via linearly constrained minimum variance spatial filtering. IEEE Trans. Biomed. Eng. 44, 867–880. https://doi.org/10.1109/10.623056

Vinck, M., Huurdeman, L., Bosman, C.A., Fries, P., Battaglia, F.P., Pennartz, C.M.A., Tiesinga, P.H., 2015. How to detect the Granger-causal flow direction in the presence of additive noise? NeuroImage 108, 301–318. https://doi.org/10.1016/j.neuroimage.2014.12.017

Vinck, M., Oostenveld, R., van Wingerden, M., Battaglia, F., Pennartz, C.M.A., 2011. An improved index of phase-synchronization for electrophysiological data in the presence of volume-conduction, noise and sample-size bias. NeuroImage 55, 1548–1565. https://doi.org/10.1016/j.neuroimage.2011.01.055

von Nicolai, C., Engler, G., Sharott, A., Engel, A.K., Moll, C.K., Siegel, M., 2014. Corticostriatal coordination through coherent phase-amplitude coupling. J. Neurosci. Off. J. Soc. Neurosci. 34, 5938–5948. https://doi.org/10.1523/JNEUROSCI.5007-13.2014

Wang, H.E., Bénar, C.G., Quilichini, P.P., Friston, K.J., Jirsa, V.K., Bernard, C., 2014. A systematic framework for functional connectivity measures. Brain Imaging Methods 8, 405. https://doi.org/10.3389/fnins.2014.00405

Zerouali, Y., Pouliot, P., Robert, M., Mohamed, I., Bouthillier, A., Lesage, F., Nguyen, D.K., 2016. Magnetoencephalographic signatures of insular epileptic spikes based on functional connectivity. Hum. Brain Mapp. 37, 3250–3261. https://doi.org/10.1002/hbm.23238

Supplementary Figures

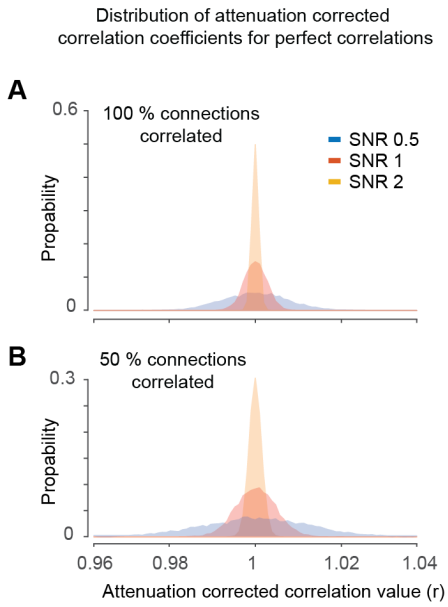

Figure S1. Simulation of attenuation corrected correlation values for perfectly correlated patterns and different noise-levels

Distribution of attenuation corrected correlations simulated for perfectly correlated patterns and added noise. The signal-to-noise (SNR) levels are set to 0.5, 1 and 2 (for further details see 2.9). The simulation is conducted for all connections (A) or half of the connections (B) being perfectly correlated with all remaining connections uncorrelated.

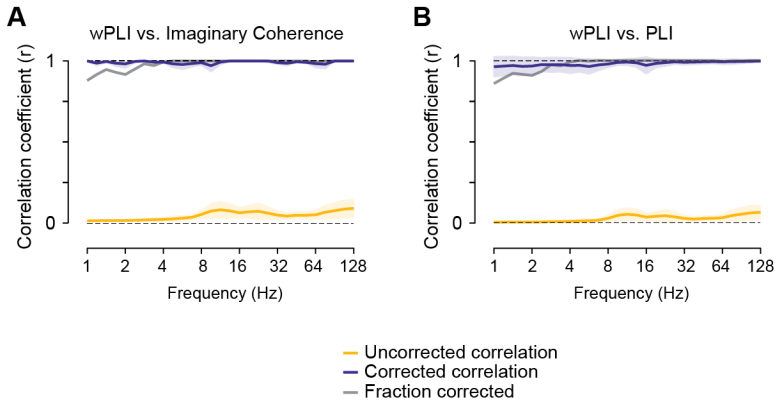

Figure S2. Comparison between different phase-coupling measures

Distribution of attenuation corrected (blue) and uncorrected (yellow) correlation between seed-patterns between the weighted phase lag index (wPLI) and imaginary coherency (ImC) (A) and between the wPLI and phase lag index (PLI) (B). The gray line indicates the relative number of corrected sources. Shaded areas indicate the standard deviation across space.